Large-Scale Sea Surface Temperature Forcing Contributed to the 2013–17 Record-Breaking Meteorological Drought in the Korean Peninsula

YOO-GEUN HAM,[a] SEON-YU KANG,[a] YERIM JEONG,[a] JEE-HOON JEONG,[a] AND TIM LI[b,c]

[a] *Department of Oceanography, Chonnam National University, Gwangju, South Korea*
[b] *International Pacific Research Center, and Department of Atmospheric Sciences, School of Ocean and Earth Science and Technology, University of Hawai'i at Mānoa, Hawaii*
[c] *Ministry of Education/Joint International Research Laboratory of Climate and Environmental Change/Collaborative Innovation Center on Forecast and Evaluation of Meteorological Disasters, Nanjing University of Information Science and Technology, Nanjing, China*

(Manuscript received 16 July 2021, in final form 11 February 2022)

ABSTRACT: This study examined the contribution of the Pacific decadal oscillation (PDO) to the record-breaking 2013–17 drought in the Korean Peninsula. The meteorological drought signal, measured by the Standardized Precipitation Index (SPI), in 2013 and 2016 co-occurred with a heat wave. The positive phase of the PDO during the mid-2010s was responsible for the precipitation deficit, particularly in 2014, 2015, and 2017, resulting in 5 years of meteorological drought. The enhanced atmospheric heating anomalies over the subtropical central Pacific, induced by the in situ PDO-related sea surface temperature (SST) warming, led to a low-atmospheric cyclonic flow centered over the midlatitude Pacific. The northerly wind anomalies at the western edge of this low-level cyclonic flow were responsible for the horizontal negative advection of moist energy, which contributed to the decreased precipitation and the resultant negative SPI over the Korean Peninsula in 2014, 2015, and 2017. The large-ensemble simulation supported the observational findings that the composited SST anomalies during the 5 years of persistent drought exhibited prominent and persistent SST warming over the subtropical central Pacific, along with large-scale cyclonic flow over the North Pacific. The findings of this study imply that the SST anomalies over the North Pacific and subtropical central Pacific can be a predictable source to potentially increase the ability to forecast multiyear droughts over the Korean Peninsula.

KEYWORDS: Climate variability; Interannual variability; Pacific decadal oscillation

1. Introduction

Drought is a natural hazard initiated by a severe and persistent deficit in precipitation (Hoerling and Kumar 2003; Hoerling et al. 2014; Seager et al. 2015). Meteorological drought, possibly combined with increased evapotranspiration, leads to soil moisture drying, which eventually leads to a soil moisture drought (Van Loon and Laaha 2015). As soil moisture depletion contributes to the attenuation of the water supply to crops, it can cause crop failure (Seager et al. 2009). In addition, the depletion of soil moisture is related to low groundwater recharge and surface runoff to streams, causing a failure of water resource systems that are essential for meeting the water demands of ecology and human society (Van Loon and Laaha 2015). Because of the impacts on various sectors such as agriculture, society, and environmental hydrology, droughts have attracted tremendous attention from environmentalists, ecologists, hydrologists, meteorologists, geologists, and agricultural scientists (Cook et al. 2010).

In particular, multiyear droughts have attracted considerable interest because of their pronounced effects on hydrology (Wu and Kinter 2009; Sattar et al. 2019) and on the occurrence of natural disasters, such as mega forest fires (Kogan and Guo 2015; Boer et al. 2020). During 2013–17, South Korea experienced a multiyear drought of a record-breaking duration and severity (Kwon et al. 2016; Bang et al. 2018). The observational data (1980–2020) showed negative values for 5 consecutive years (2013–17), which was the longest drought over the last 40 years (Figs. 1a,b). The record-breaking duration of the drought event during the corresponding years is still observed by following the detection method using multiple hydrological variables (i.e., precipitation and soil moisture; Mo 2011) (not shown). The drought severity, measured by the accumulated negative precipitation during the drought duration, also exhibited a maximum value over the last 40 years (Fig. 1c). The drought signal in the central district of South Korea, where the metropolitan area is located, was even more severe in terms of both duration and severity (Figs. 1a and 2).

The record-breaking 2013–17 drought signals in the Korean Peninsula were moderate in 2013, 2014, and 2016 and the strongest in 2015 and 2017. In the central district of South Korea, the drought signals in 2014 and 2015 were the strongest (Fig. 1a). Specifically, during the summer of 2014, the amount of precipitation in South Korea was approximately 50% of the climatological amount. The amount of precipitation over South Korea was 85%, 72%, and 59% of the climatological amount during the boreal winter of 2014/15, spring 2015, and summer 2015, respectively. The precipitation deficit for 3 consecutive years over 2013–15 led to serious water storage deficits in the summer of 2015. In June 2015, the Soyang Dam, which is the largest dam in the central district of South Korea and the major supplier of electricity for the metropolitan area, recorded the lowest water level since its construction in 1973. The cumulative precipitation from January to May 2017 was 181.5 mm, which is less than half of the average

Corresponding author: Yoo-Geun Ham, ygham@jnu.ac.kr

DOI: 10.1175/JCLI-D-21-0545.1

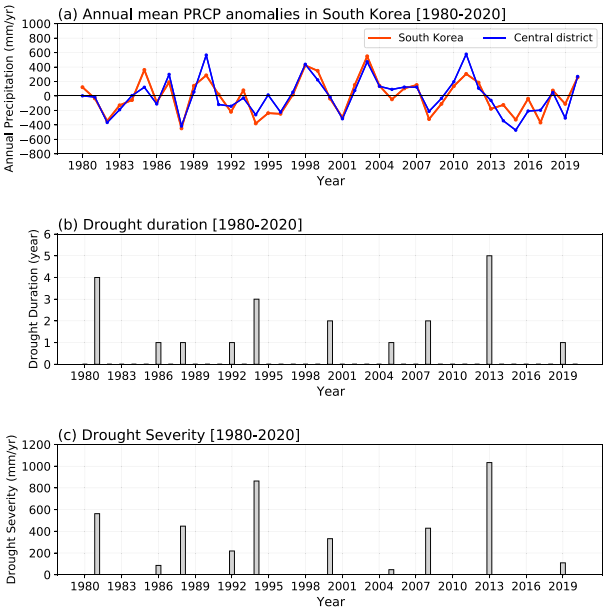

FIG. 1. (a) The detrended annual-mean station-based precipitation anomalies over South Korea (red) and just the central district of South Korea (blue) during 1980–2020. (b) Duration and (c) severity of the drought events over South Korea during 1980–2020. The values on the x axis denote that the start year of drought events with the corresponding drought duration. To obtain the detrended anomaly, the linear trend during 1980–2020 was removed. The drought duration is defined as the number of consecutive years with the negative detrended annual-mean precipitation anomalies. The drought severity is determined as the accumulated rainfall deficit over the corresponding duration.

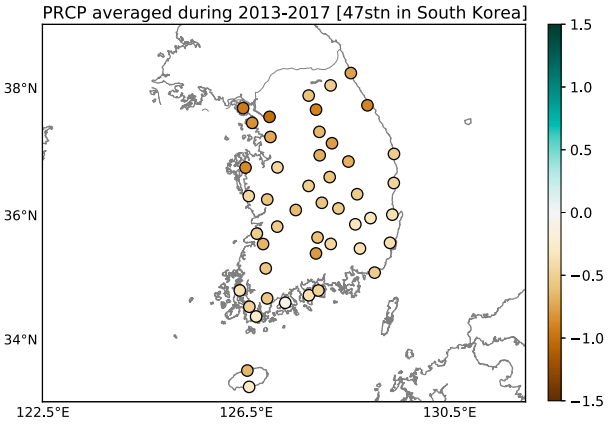

FIG. 2. The 5-yr-averaged precipitation anomalies during 2013–17 at the 47 stations in South Korea used in this study.

value during 1981–2010 for this period, the second lowest precipitation since 1973 (Bang et al. 2018).

In North Korea, the economic damage caused by the 2013–17 drought was even greater, owing to the lack of infrastructure. In 2015, grain and rice production in North Korea decreased by 18% and 21%, respectively, compared to the previous year's production due to drought damage (Nam et al. 2017). Due to this damage, North Korea openly declared a food shortage through the state media and requested international assistance in 2015. The Global Information and Early Warning System on Food and Agriculture noted a crisis of food security caused by extreme drought over North Korea in 2017 (Deng et al. 2018).

Land–atmosphere interaction can intensify the severity of a multiyear drought and prolong its duration (Fischer et al. 2007; Roundy et al. 2013; Zeng et al. 2019). Reduced soil moisture tends to decrease evapotranspiration and subsequent precipitation suppression to prolong drought persistence (i.e., positive soil moisture–precipitation feedback) (Findell and Eltahir 1997; Eltahir 1998; Pal and Eltahir 2001; Wu and Kinter 2009). Moreover, a large soil moisture deficit, led by a precipitation deficit, reduces latent cooling and increases the near-surface temperature. Surface temperature warming exerts heat to the atmosphere in the form of sensible heat flux to raise the atmospheric boundary layer (Fischer et al. 2007; Santanello et al. 2011) and induce high pressure anomalies (Wang et al. 2015). This further strengthens and prolongs drought (i.e., positive soil moisture–surface temperature feedback). Recent soil drying caused by global warming has enhanced this land–atmosphere coupling to increase the occurrence of droughts over East Asia (Zhang et al. 2020).

Although land–atmosphere coupling is known to contribute to drought duration and severity, it cannot initiate drought signals. Instead, the drought signal, represented by a precipitation deficit, tends to be initiated by a certain remote teleconnection pattern, which is called the stationary wave pattern (Schubert et al. 2011, 2014). For example, Wang et al. (2017) attributed the 2015 summer North China drought to a quasi-stationary wave train called the Eurasian pattern (Wallace and Gutzler 1981). Wang and He (2015) argued that the July–August 2014 drought over northeastern Asia was jointly caused by the Silk Road pattern (Lu et al. 2002) and Pacific–Japan pattern (Nitta 1987; Kosaka and Nakamura 2006).

These stationary wave patterns are often excited by large-scale sea surface temperature (SST) forcing (Seager and Hoerling 2014). Many studies have demonstrated that stationary wave trains responsible for droughts in the United States are induced by a cold eastern tropical Pacific (Schubert et al. 2008; Wang and Schubert 2014). Seager et al. (2015) analyzed the causes of the California drought during November–April of 2011/12 and 2013/14 and found that SST forcing was key to sustaining a high pressure ridge over the west coast of the United States and suppressing precipitation.

Although the relationship between tropical SST forcing and the precipitation deficit over East Asia has been investigated, most of these studies were based on a linear analysis targeted on a specific season (Jin et al. 2005; Ha et al. 2010; Lee and Julien 2016; Ham et al. 2016; Yeh et al. 2018). The cyclonic flow over the Philippine Sea, which develops during the mature La Niña phase, plays a critical role in reducing the amount of precipitation over Asian countries located in subtropical regions (Wang et al. 2000; Li et al. 2018). And it has

TABLE 1. The ID and geological location of the 47 stations in South Korea provided by the Korea Meteorological Agency (KMA).

ID	Station No.	Station name	Lon (°E)	Lat (°N)	ID	Station No.	Station name	Lon (°E)	Lat (°N)
1	90	Sokcho	128.56	38.25	25	212	Hongcheon	127.88	37.68
2	101	Chuncheon	127.73	37.90	26	221	Jecheon	128.19	37.15
3	105	Gangneung	128.89	37.75	27	226	Boeun	127.73	36.48
4	108	Seoul	126.96	37.57	28	232	Cheonan	127.29	36.76
5	112	Incheon	126.62	37.47	29	235	Boryeong	126.55	36.32
6	114	Wonju	127.94	37.33	30	236	Buyeo	126.92	36.27
7	119	Suwon	126.98	37.27	31	238	Geumsan	127.48	36.10
8	127	Chungju	127.95	36.97	32	243	Buan	126.71	35.72
9	129	Seosan	126.49	36.77	33	245	Jeongeup	126.83	35.56
10	130	Uljin	129.41	36.99	34	260	Jangheung	126.91	34.68
11	135	Chupungnyeong	127.99	36.22	35	261	Haenam	126.56	34.55
12	138	Pohang	129.38	36.032	36	262	Goheung	127.27	34.61
13	143	Daegu	128.65	35.82	37	272	Yeongju	128.51	36.87
14	146	Jeonju	127.11	35.84	38	273	Mungyeong	128.14	36.62
15	152	Ulsan	129.32	35.56	39	277	Yeongdeok	129.40	36.53
16	156	Gwangju	126.89	35.17	40	278	Uiseong	128.68	36.35
17	159	Busan	129.03	35.10	41	279	Gumi	128.32	36.13
18	165	Mokpo	126.38	34.81	42	281	Yeongcheon	128.95	35.97
19	168	Yeosu	127.74	34.73	43	284	Geochang	127.91	35.67
20	170	Wando	126.70	34.39	44	285	Hapcheon	128.16	35.56
21	184	Jeju	126.52	33.51	45	288	Miryang	128.74	35.49
22	189	Seogwipo	126.56	33.24	46	289	Sancheong	127.87	35.41
23	201	Ganghwado	126.44	37.70	47	295	Namhae	127.92	34.81
24	211	Inje	128.16	38.05					

been found that summer rainfall over the Korean Peninsula tends to decrease during La Niña events (Kug et al. 2010; Son et al. 2016; Park et al. 2020). The development of the cyclonic flow over the Kuroshio Extension region is the main link connecting La Niña and reduced precipitation over the Korean Peninsula during the boreal winter season (Son et al. 2014). In addition, large-scale SST variability over the Indian Ocean (Kim and Kug 2021), the off-equatorial western Pacific (Wu et al. 2010; Ham et al. 2016), the equatorial Atlantic (Ham et al. 2017, 2018), and the North Atlantic (Sung et al. 2006; Myoung et al. 2020) affect precipitation over the Korean Peninsula by inducing large-scale atmospheric variability, such as the circumglobal teleconnection pattern (Ding and Wang 2005), the Pacific–Japan pattern (Nitta 1987; Kosaka and Nakamura 2006), and summer North Atlantic Oscillation (Folland et al. 2009; Osborne et al. 2020).

However, the link between SST forcing and various types of droughts over East Asia is not clearly understood and it has not been determined whether SST forcing was responsible for the multiyear persistent precipitation deficit during 2013–17 over the Korean Peninsula. Therefore, this study was conducted to determine the large-scale SST signal that contributed to the 2013–17 drought over the Korean Peninsula. The data and methodology are presented in section 2. Section 3 describes the categorization of the 2013–17 drought in the Korean Peninsula. Sections 4 and 5 investigate the large-scale SST forcing responsible for the 2013–17 drought. Section 6 reports the results of a long-term climate model simulation with large ensemble members. The main findings are summarized in section 7.

2. Data

a. Observational data

The monthly mean SST, 850-hPa zonal and meridional wind, and soil moisture data were derived from the European Center for Medium-Range Weather Forecasts (ECMWF) ERA5 reanalysis (Hersbach et al. 2020). The dataset was interpolated at a spatial resolution of 2.5° × 2.5° using the bilinear interpolation method (Press et al. 1986), except for the total soil column moisture data, with a finer original resolution (0.5° × 0.5°), which was used to diagnose the soil wetness over the Korean Peninsula. The monthly precipitation data were derived from version 2.3 of the Global Precipitation Climatology Project (GPCP; Adler et al. 2018) on a 2.5° resolution grid. We utilized station-based precipitation and near-surface air temperature monthly data (1980–2020; 41 years) from 47 stations over South Korea. This dataset was provided by the Korea Meteorological Administration (KMA) (https://data.kma.go.kr/data/grnd/selectAsosRltmList.do?pgmNo=36). The geological locations of the 47 stations are given in Table 1.

To diagnose the meteorological drought condition during 2013–17, 3- and 12-month versions of the Standardized Precipitation Index (SPI; referred to as SPI-3 and SPI-12 respectively) were generated from 3- and 12-month averaged precipitation data, respectively. SPI is a widely used index to characterize meteorological drought on a range of time scales (Hayes et al. 1999; Vautard et al. 2007; Fischer et al. 2007), even though it does not consider the dynamical propagation to soil moisture and hydrological drought (Van Loon and Laaha 2015). The raw precipitation data were fitted to a gamma distribution and then transformed to a normal

distribution. The SPI values can be interpreted as the number of standard deviations by which the observed anomaly deviates from the long-term mean. The SPI-12 was defined using 12-month averaged precipitation from January to December for each year to diagnose each year's drought condition. The SPI-3 for each season was calculated using the precipitation data for the corresponding three months, and then utilized to assess the drought signal corresponding to the seasonal climate variation. For example, SPI-3 for the March–May (MAM) season was calculated using three months of precipitation during MAM. We removed the linear trend of the SPI during 1980–2020 before the analysis.

The monthly Pacific decadal oscillation (PDO) index (Mantua et al. 1997) was downloaded from the National Centers for Environmental Information (https://www.ncdc.noaa.gov/teleconnections/pdo/). The monthly Pacific meridional mode (PMM) index (Chiang and Vimont 2004) was downloaded from the National Oceanic and Atmospheric Administration Physical Sciences Laboratory (https://psl.noaa.gov/data/timeseries/monthly/PMM/). The period of all indices was 1980–2020. The monthly climatological value and the linear trend during 1980–2020 were subtracted to calculate the detrended anomaly. The PDO and PMM indices were normalized by dividing the standard deviation during 1980–2020 at the corresponding calendar month.

b. *Model output*

We used the Community Earth System Model version 2 with large ensemble members (referred to as CESM2 LE) during 1850–2014 (Rodgers et al. 2021), which builds on the successes of its previous version (Danabasoglu et al. 2020). The climatological bias in the global precipitation, temperature, and radiative forcing in CESM2 LE is significantly lower than that in CESM1. Capotondi et al. (2020) mentioned that the overall spatial distribution of the Pacific decadal variability was similar to observed values. CESM2 accurately simulates several aspects of El Niño–Southern Oscillation (ENSO), including dominant time scale, tropical and extratropical precursors, composited time evolution, and teleconnection (Capotondi et al. 2020). The seasonal timing of the South Asian monsoon, monsoon–ENSO connections, and monsoon intraseasonal variability are simulated better than those simulated by CESM1 (Meehl et al. 2020). In addition, the quality of simulating Northern Hemisphere storm tracks, stationary waves, and blocking ranks within the top 10% of CMIP class models (Simpson et al. 2020). These references indicate that the CESM2 LE is one of the best choices for analyzing the role of large-scale oceanic climate variability on the Northern Hemisphere midlatitude meteorological drought.

Among total 100 members, we utilized the first 50 members that followed the CMIP6 protocol with biomass burning (Rodgers et al. 2021). The remaining 50 ensemble members are not utilized in this study due to the possible systematic difference led by different biomass burning protocol. The model was interpolated at a resolution of $2.5^\circ \times 2.5^\circ$ using a bilinear interpolation method. The monthly mean SST, precipitation, and 850-hPa zonal and meridional wind were utilized.

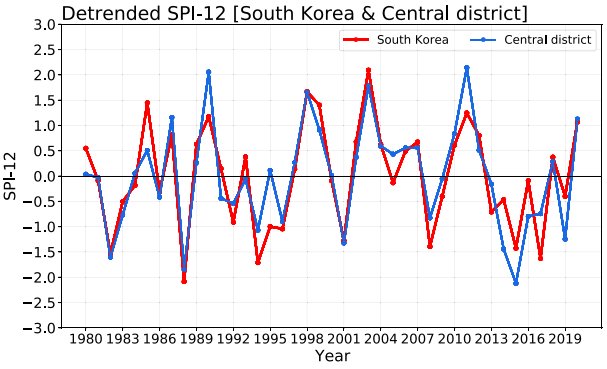

FIG. 3. Detrended SPI-12 over South Korea (red) and just the central district of South Korea (blue). Note that the SPI-12 for any particular year is calculated by using the 12-month precipitation from January to December of the corresponding year.

To define the modeled SPI index, we used a wider area (i.e., land area-averaged value over 30°–50°N, 110°–140°E) than that covered by the observational analysis, as global climate models have a modest horizontal resolution that might not be capable of detecting the large-scale climate signals associated with the relatively narrow East Asian region. We defined the multiyear drought event as the period when the annual mean precipitation exhibited negative values for 5 consecutive years as in 2013–17 drought, and its initiation was defined as the first month when monthly precipitation became negative. A total of 114 multiyear drought events were identified among 165 years of data with 50 ensemble members (i.e., a total of 8250 years). Among them, 95% of multiyear droughts were initiated during the boreal spring (i.e., February, March, or April), similar to the initiation of the 2013–17 drought (in April 2013). To consider the seasonality of the multiyear drought, only events that were initiated in February, March, and April were used for the analysis.

To determine the PDO index in the CESM2 LE, we used monthly SST anomalies after removing the global mean SST anomalies in the corresponding month (Mantua and Hare 2002). The PDO index was defined as the principal component of the leading empirical orthogonal function (EOF) over the region 20°–70°N, 120°E–110°W.

3. Categorization of 2013–17 multiyear drought in the Korean Peninsula

Figure 3 shows the detrended SPI-12 during 1980–2020 over South Korea and the central district of South Korea. A negative SPI-12 is evident over South Korea during 1982–84, 1986, 1988, 1992, 1994–96, 2001, 2008–09, 2013–17, and 2019, denoting the drought signal during the corresponding years. Among them, the 2013–17 drought event was the longest. The SPI-12 over the central district of South Korea also exhibited negative values for the longest period during 2013–17, with that in 2014 being the lowest of the last 40 years, indicating that the 2013–17 drought event is one of the most severe drought events over the last 40 years in South Korea.

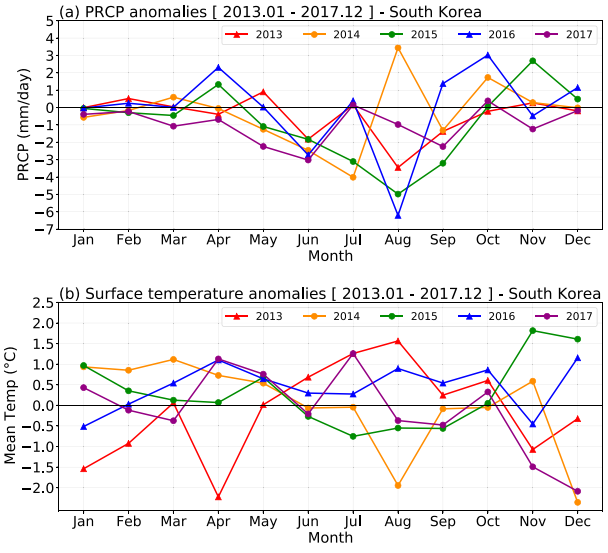

FIG. 4. The station-based detrended monthly (a) precipitation and (b) surface temperature anomalies over South Korea during 2013–17.

To examine the detailed time evolution of the drought signal during 2013–17, Fig. 4a shows the observed monthly precipitation anomalies over South Korea. In 2013, negative precipitation anomalies were induced in April that continued up to October. In 2014, negative precipitation anomalies occurred in April and were sustained up to September except for the strong positive anomalies in August. In 2015, the negative precipitation anomalies that developed in May, exhibited the second greatest magnitude in August over the 5 years. Negative precipitation anomalies were observed in 2016 at June and August with the strongest magnitude in August among the 5 years. On the other hand, the precipitation deficit in 2016 was canceled by the positive precipitation anomalies during the boreal spring and winter seasons. Negative precipitation anomalies in 2017 continued from February to December.

The drought signal during 2013–17 can be categorized into two groups based on the intensification rate of the precipitation deficit during the boreal summer season. In group 1, in 2013 and 2016 (lines with triangles) the amplitude of negative precipitation anomalies rapidly increased from May to June. For example, the precipitation anomaly in May 2013 was $+1$ mm day^{-1}, and it abruptly changed to -1.7 mm day^{-1} in June. Similarly, the precipitation anomaly in May 2016 was nearly zero, but reached approximately -2.8 mm day^{-1} in July 2016. In addition, in 2013 and 2016, the precipitation deficit exhibited a sharp second peak in August. In group 2, on the other hand, in 2014, 2015, and 2017 (lines with circles) the precipitation deficit gradually enhanced during the boreal summer season. This implies that the drought signals in 2013 and 2016 were caused by a different mechanism from those in 2014, 2015, and 2017.

To examine the differences in the mechanisms of drought in 2013 and 2016 from those in 2014, 2015, and 2017 in more detail, Fig. 4b shows the station-based detrended monthly near-surface temperature anomalies over South Korea. The most distinctive feature of the drought signal in 2013 and 2016 was the co-occurrence of a precipitation deficit with positive surface temperature anomalies. In 2013, negative precipitation anomalies abruptly developed during the boreal summer season, with the co-occurrence of positive surface temperature anomalies. Similarly, in 2016, positive surface temperature anomalies occurred in June–August (JJA). On the other hand, the positive near-surface surface temperature anomalies were not robust during the boreal summers of 2014, 2015, and 2017, and they even exhibited negative values in most boreal summer seasons. This indicates that the drought signal during 2013–17 can be divided into two groups: 2013 and 2016, which co-occurred with a heat wave during boreal summer, and 2014, 2015, and 2017, which were induced separately from the heat wave.

The co-occurrence of heat waves and droughts has recently received increasing attention (Peters et al. 2002; Mo and Lettenmaier 2015). High geopotential height anomalies can initiate heat waves and droughts simultaneously by increasing shortwave radiation and suppressing precipitation, respectively (Wang and Yuan 2018). As an extremely positive surface temperature anomaly can amplify the high pressure anomalies by increasing the sensible heat flux to thicken the planetary boundary layer (Zhang et al. 2020), the heat wave signal contributes to the maintenance and amplification of a drought.

The causes of the high geopotential height anomalies that initiated the heat waves and drought signals in 2013 and 2016 are relatively well known. Xia et al. (2016) reported that the 2013 heat wave in eastern China was caused by record-breaking and multidecadal variability over the North Pacific, which led to the abnormal development of the western Pacific subtropical high (Peng 2014). For the heat wave in 2016, Yeh et al. (2018) showed that the anomalously high geopotential height over the Korean Peninsula in August 2016 was triggered by strong convection in the western-to-central subtropical Pacific. This finding is similar to that of Yeo et al. (2019), who determined that the meridionally propagated atmospheric teleconnection pattern excited by the enhanced convection over the tropical western Pacific around the Maritime Continent induces heat wave-related high geopotential height anomalies. Those aforementioned studies indicate that the mechanism of the heat wave-coupled drought signal in 2013 and 2016 is also understood to some extent. However, as mentioned in section 1, the factors contributing to the 2013–17 drought signal, which caused the precipitation deficit in 2014, 2015, and 2017, have not been examined. Therefore, in the next section, we clarify the large-scale SST forcing responsible for the drought signal in 2014, 2015, and 2017.

4. Large-scale factors that induced drought signals in 2014, 2015, and 2017

Figure 5 shows the spatial distribution of the detrended SPI-3 and 3-month-averaged geopotential height at 850 hPa from December–February (DJF) to September–November (SON) in 2014, 2015, and 2017. During DJF 2013/14, negative

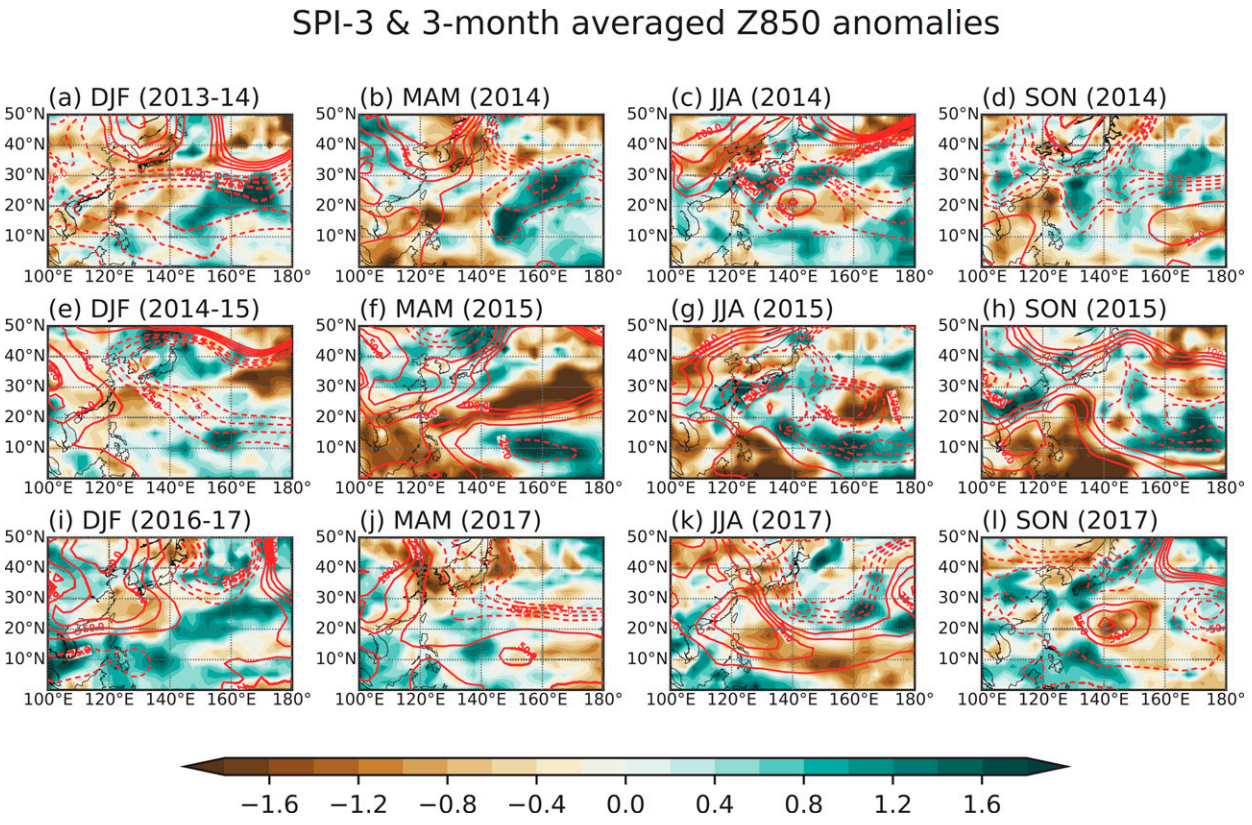

FIG. 5. Spatial distribution of SPI-3 and 3-month-averaged Z850 anomalies during (a) DJF 2013/14, (b) MAM 2014, (c) JJA 2014, (d) SON 2014, (e) DJF 2014/15, (f) MAM 2015, (g) JJA 2015, (h) SON 2015, (i) DJF 2016/17, (j) MAM 2017, (k) JJA 2017, and (l) SON 2017.

SPI-3 mainly occurred to the south of the Korean Peninsula and Japan, and over the Yangtze River Basin (Fig. 5a). On the other hand, positive precipitation anomalies occurred over the western Pacific at 10°–30°N, 140°–180°E. This dipole structure of precipitation anomalies was also clear during MAM 2014 (Fig. 5b). During JJA 2014, the negative SPI-3 was particularly strong over the Korean Peninsula, Japan, and northern China (Fig. 5c). The negative SPI-3 was maintained over the Korean Peninsula until SON 2014 and DJF 2014/15, whereas the SPI-3 over Japan and China exhibited positive values those seasons (Figs. 5d,e).

Negative SPI-3 also occurred over the Korean Peninsula in 2015, particularly during JJA (Figs. 5f–h). During MAM 2015, negative SPI-3 only occurred over the central district of South Korea, and its amplitude was lower than that in other seasons. However, during JJA 2015, its amplitude intensified and extended to northern China. The negative SPI-3 signal over the Korean Peninsula also steadily occurred from MAM to SON in 2017 (Figs. 5i–l).

The large-scale circulation anomaly is responsible for the precipitation anomalies over East Asia, including the drought signal over the Korean Peninsula. During most seasons in 2014, 2015, and 2017, large-scale negative geopotential height anomalies were prominent over the western Pacific (red dotted contours in Fig. 5). Over the western edge of the low geopotential height anomaly, northerly winds advect cold and dry air from higher latitudes, which reduce precipitation over the Korean Peninsula (Ham et al. 2007). At the center of the low geopotential height anomalies, precipitation tends to increase owing to low-level atmospheric convergence. Therefore, a dipole pattern is commonly observed for the precipitation response (Ham et al. 2016). In addition, during the boreal summer, low geopotential height anomalies over the western Pacific are linked to the attenuation of the northward extension of the climatological high, and the resultant southward shift of the mei-yu–baiu–changma front is responsible for the decreased and increased precipitation anomalies over the Korean Peninsula and south of Japan, respectively (Figs. 5c,g). During the boreal winter season of 2015 and 2017 (Figs. 5e,i), the northern part of the negative geopotential height anomalies is associated with the southward expansion of the East Asia trough (Wang et al. 2009), which increases the precipitation.

To reveal the large-scale SST forcing responsible for the drought signal in 2014, 2015, and 2017, the seasonal SST anomalies from DJF 2013/14 to SON 2017 were calculated, as shown in Fig. 6. During DJF 2013/14, negative SST anomalies occurred over the equatorial central Pacific. These anomalies became positive during MAM 2014, indicating the initiation of an El Niño event. However, this event abruptly weakened during JJA 2014, even though the positive SST anomaly restrengthened during SON 2014. The amplitude of the El

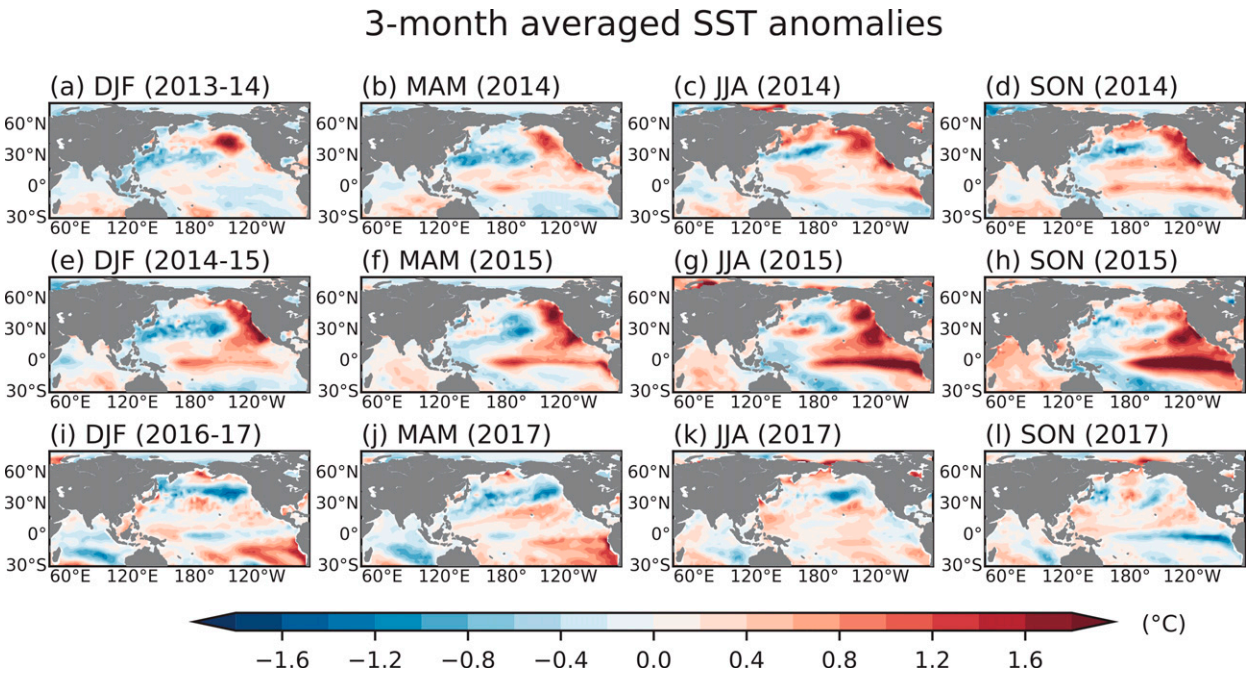

FIG. 6. As in Fig. 5, but for SST anomalies.

Niño event during the DJF 2014/15 indicates moderate warming (Min et al. 2015; Hu and Fedorov 2016; Dong and McPhaden 2018). In contrast, the strength of El Niño, which was suspended in 2014, increased rapidly in 2015. The continuous warming of the prominent SST anomalies over the equatorial Pacific in 2015 led to one of the strongest El Niño events in the boreal winter of 2015/16 (Lim et al. 2017; Newman et al. 2018; Kim and Yu 2020). The SST anomalies over the equatorial eastern Pacific exhibited weak values from DJF 2016/17 to JJA 2017, and turned negative during SON 2017. As a result, the ENSO signals differed significantly in 2014, 2015, and 2017. Similarly, the SST anomalies over the Indian Ocean were quite different from those in 2014, 2015, and 2017. Indian Ocean SST warming, which tends to occur with El Niño events (Klein et al. 1999; Xie et al. 2002; Li et al. 2003), was prominent during the boreal summer and autumn of 2015; however, no systematic SST anomaly signal was observed in 2014 and 2017.

In contrast, the spatial distribution of SST anomalies over the North Pacific exhibited some similarities among 2014, 2015, and 2017. The horseshoe pattern of positive anomalies over the eastern North Pacific and subtropical central Pacific along with the negative anomalies over the western–central North Pacific developed in MAM 2014, and was then sustained until SON 2015. Although positive SST anomalies over the eastern North Pacific were not evident in 2017, the subtropical loading of the positive SST anomalies over the central Pacific and the negative SST anomalies over the western–central North Pacific were evident throughout 2017. The spatial distribution of SST anomalies over the North Pacific resembled that of the positive phase of the PDO (Di Lorenzo and Mantua 2016) or PMM (Chiang and Vimont 2004; Chang et al. 2007). The time series of PDO and PMM indices generally support our finding that a positive PDO or PMM event occurred during 2014, 2015, and 2017 (Fig. 7).

The possible role of PDO-related SST forcing on climate variability in the Korean Peninsula has been reported previously. Kim et al. (2014) and Lee et al. (2019) found that the correlation between the typical PDO pattern and the climate variability over the Korean Peninsula is quite weak [see, e.g., Fig. 3 of Lee et al. (2019)]; however, the modulation of PDO by other climatic variability (i.e., ENSO in their study) can lead to significant climatic variations over the Korean Peninsula. Similar to their findings, this study demonstrates that the westward extension of SST warming over the subtropical

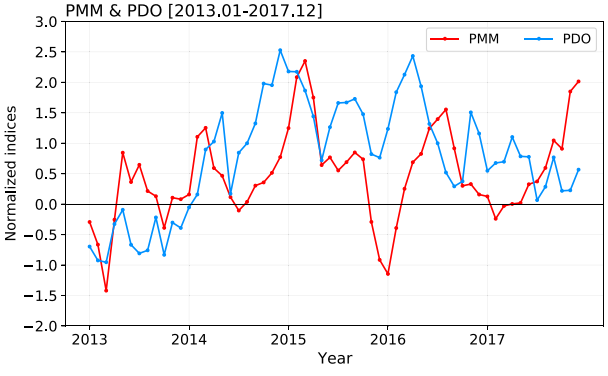

FIG. 7. Normalized monthly time series of the Pacific decadal oscillation (PDO) and Pacific meridional mode (PMM) indices from January 2013 to December 2017. The time series is normalized by dividing its standard deviation during 1980–2020 at the corresponding calendar month.

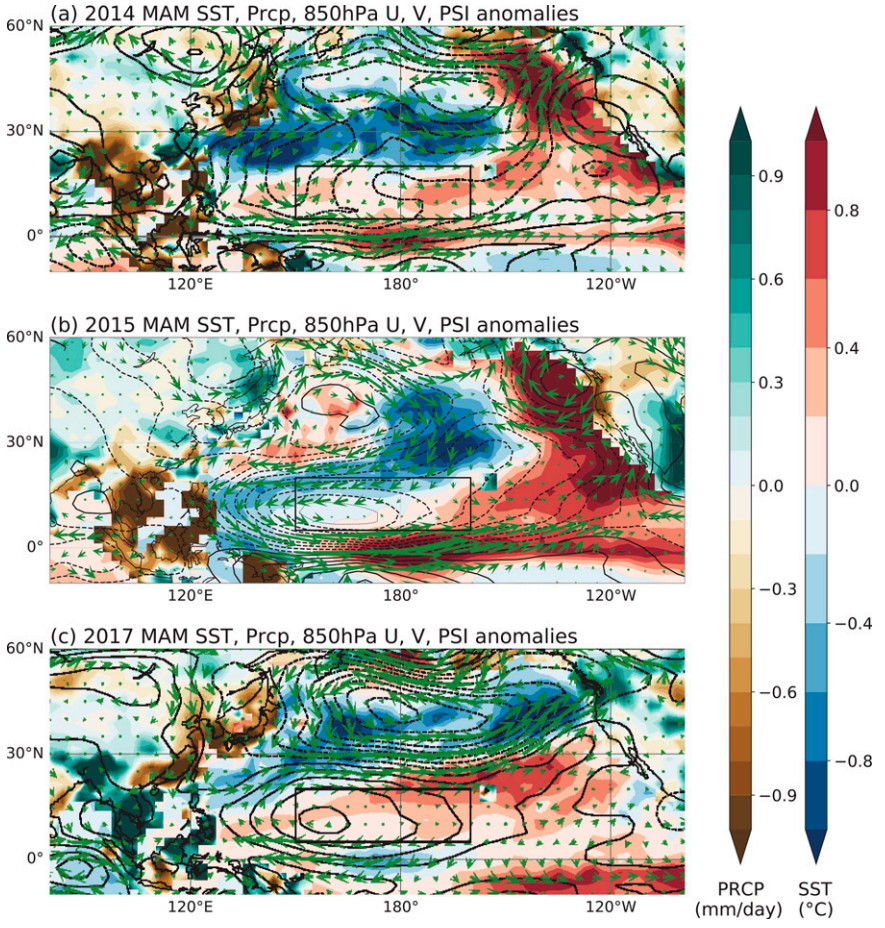

FIG. 8. Spatial distribution of SST (shading over the ocean; unit: °C), precipitation (shading over the land; unit: mm day^{-1}), 850-hPa wind vector (arrows; unit: m s^{-1}), and 850-hPa streamfunction (contours; unit: 10^6 m^2 s^{-1}) anomalies during (a) MAM 2014, (b) MAM 2015, and (c) MAM 2017. The black box denotes the area to define the SubTCP index (i.e., 5°–20°N, 150°E–160°W).

central Pacific modulated typical PDO patterns, which is a key to the PDO-related North Pacific variability that led to the drought signal in 2014, 2015, and 2017 over the Korean Peninsula.

5. Contribution of the PDO-related subtropical SST warming over the central Pacific to the 2013–17 drought event in the Korean Peninsula

The hypothesis that the PDO-related SST anomalies play an important role in the 2013–17 drought event in the Korean Peninsula can be confirmed by understanding the detailed mechanisms involved. We compared the detailed SST pattern with the associated atmospheric responses in 2014, 2015, and 2017 to determine how climatic forcing associated with the positive PDO event contributed to the 2013–17 drought in the Korean Peninsula.

Figure 8 shows the SST, precipitation, and 850-hPa wind anomalies during MAM in 2014, 2015, and 2017. We selected MAM as this is when both the PDO and PMM indices tend to exhibit a maximum value in 2014, 2015, and 2017 (Fig. 7). In the plot of SST anomalies for MAM 2014 and 2015, the negative SST anomalies over the western North Pacific and the horseshoe pattern of positive SST anomalies over the subtropical central Pacific and eastern North Pacific are clearly visible. The positive SST anomalies over the subtropical central Pacific leads the in situ positive precipitation anomalies. These positive precipitation anomalies infer that the larger amount of water vapor than the climatology turned into the liquid water, and this water phase change leads the additional heat release in the atmosphere. While the east–west contrast pattern is not clear in MAM 2017, substantial negative SST anomalies existed over the entire North Pacific, and the southern loading of the horseshoe pattern of positive SST anomalies is clear over the eastern Pacific at 5°–30°N.

In MAM 2014, the lower-tropospheric cyclonic circulation covered most of the northern Pacific north of 10°N. It can also be interpreted as a Gill-type response to the atmospheric

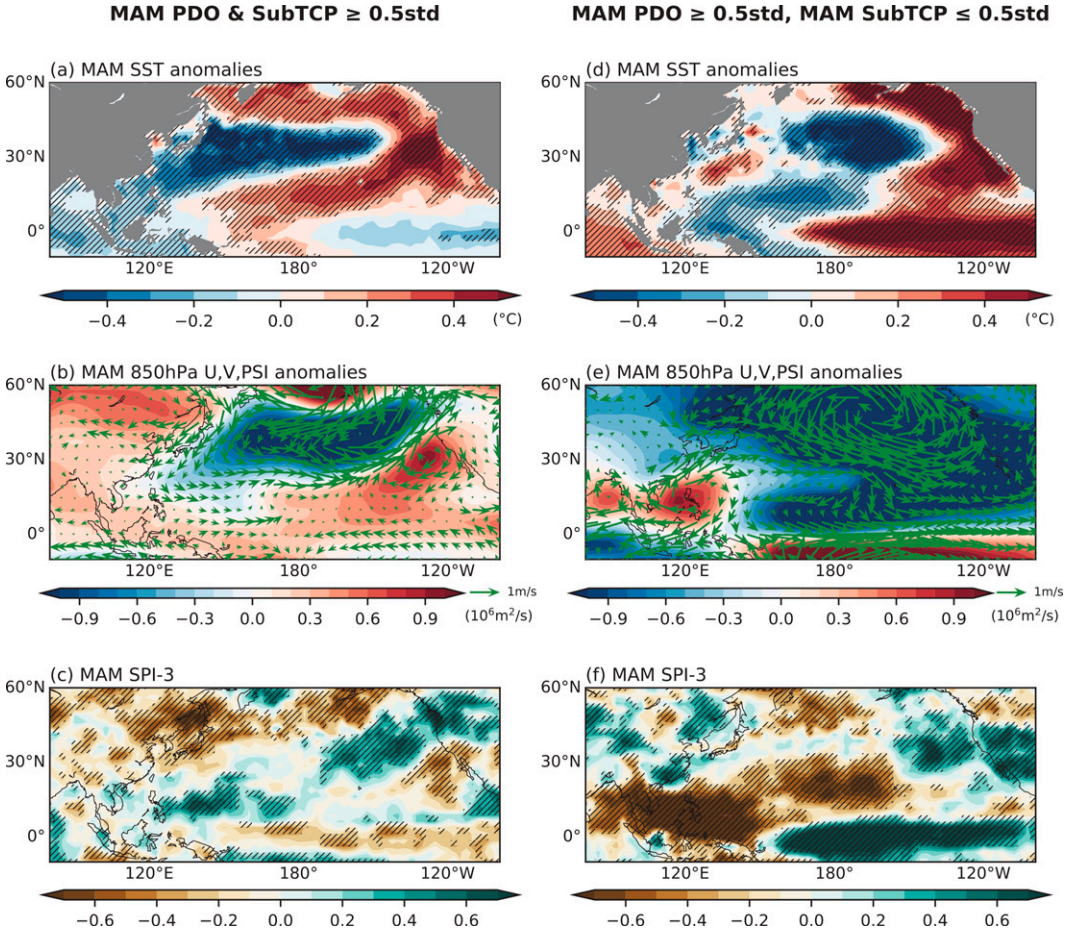

FIG. 9. (a) SST anomalies, (b) 850-hPa horizontal wind vectors and streamfunction anomalies, and (c) SPI-3 during MAM during the positive PDO events with off-equatorial central Pacific SST warming (i.e., the SubTCP index defined as an area-averaged SST over 5°–20°N, 150°E–160°W > 0.5 std). Also shown are the (d) SST, (e) 850-hPa horizontal wind and streamfunction, and (f) SPI-3 during MAM during the positive PDO events without off-equatorial central Pacific SST warming (i.e., SubTCP index < 0.5 std).

heating over the subtropical Pacific caused by local SST warming (Gill 1980; Kim and Kug 2019). Once the cyclonic circulation anomalies are induced, the southwesterlies over the region of SST warming reduce the wind speed and the resultant latent heat flux to reintensify subtropical SST warming (Wang et al. 2000; Chiang and Vimont 2004). The northerly wind associated with this cyclonic circulation was dominant over the Korean Peninsula and Japan, which advected relatively cold and dry air from the north. This negative moist energy advection reduces the precipitation amount (Ham et al. 2007; Park et al. 2020; Zhang et al. 2021). These circulation anomalies were also evident in MAM 2017, even though the overall cyclonic circulation shifted to the north, possibly due to the northward shift of the southern loading of the horseshoe pattern of positive SST anomalies and negative SST anomalies over the North Pacific.

The horizontal scale of the lower-tropospheric cyclonic flow in MAM 2015 was not as large as that in 2014 or 2017. The cyclonic flow was confined to the subtropical western–central Pacific and the eastern North Pacific, while an anticyclonic flow occurred over the western North Pacific. As a result, the amplitude of the northerly wind was quite weak over the Korean Peninsula, which led to weak negative precipitation anomalies.

The spatial pattern of SST anomalies in 2014 and 2017 show a systematic difference in the degree of westward extension of the southern loading of the positive POD-related SST anomalies compared to that in 2015. That is, in 2014 and 2017, the positive SST anomalies extended from the subtropical eastern to western Pacific, while those in 2015 were confined to the subtropical eastern Pacific. Differences in the degree of subtropical SST warming can result in different atmospheric circulation responses: there were low geopotential height anomalies over the entire North Pacific in 2014 and 2017, while the anomalies in 2015 were confined to the eastern North Pacific. As a result, the northerly over the Korean Peninsula, along with the precipitation deficit, was relatively strong in MAM 2014 and 2017. On the other hand, the precipitation

deficit led by northerly winds was also relatively weak in MAM 2015.

To support our notion that positive SST anomalies over the subtropical central Pacific played an important role in the 2013–17 drought over the Korean Peninsula, we categorized the PDO events into two groups. First, we defined the subtropical central Pacific SST index (referred to as the SubTCP index) as the area-averaged SST over 5°–20°N, 150°E–160°W (black box in Fig. 8). In MAM, both the PDO and SubTCP indices exceeded 0.5 standard deviation (std) (defined as cases with positive PDO events with a positive SubTCP index). For comparison, positive PDO events without a positive SubTCP index occurred when the PDO index was >0.5 std and SubTCP index <0.5 std. Between 1980 and 2020, there were 8 years with a positive PDO event and a positive SubTCP index (1982, 1986, 1988, 1995, 1996, 1997, 2003, and 2014) and seven positive PDO events without a positive SubTCP index (1980, 1990, 1994, 2015, 2016, 2018, and 2019).

Figure 9 compares the MAM SST, 850-hPa streamfunction, and SPI-3 during positive PDO events with and without a positive SubTCP index. Both groups had robust positive PDO signals but exhibited clear differences in SST anomalies over the subtropical central Pacific. In positive PDO events with positive SubTCP warming, the cyclonic circulation (i.e., negative streamfunction anomaly) was overwhelmed over the North Pacific. As a result, northerly winds were dominant in the Korean Peninsula, which decreased the SPI-3. This is similar to the situation in MAM 2014 and 2017 when the SPI-3 over the Korean Peninsula exhibited a negative value with a significant positive SubTCP index (i.e., normalized MAM SubTCP index in 2014 and 2017 was 1.01 and 1.08, respectively).

In contrast, during positive PDO events without a positive SubTCP index, cyclonic circulation was confined over the central–western North Pacific and failed to expand to East Asia. The overall pattern was similar to that in MAM 2015 when SPI-3 over the Korean Peninsula exhibited a nearly zero value with a low SubTCP value (i.e., normalized SubTCP value was 0.11). It should be noted that as the amplitude of dipole SST anomalies over the North Pacific is stronger during PDO events without a positive SubTCP index, the expansion of the PDO signal to the subtropical central Pacific, rather than the PDO intensity, is the key to link the PDO to East Asian climate variability.

Then, what is the role of the PDO itself on the 2013–17 drought in the Korean Peninsula? First, the PDO is one of the dominant climatic variabilities that can induce SubTCP warming. Figure 10a shows the lag correlation between the PDO index during MAM and the SubTCP index. The positive lag correlation between the PDO index and the SubTCP index was statistically significant after a lag of 3 months, which implies that PDO is one of the dominant North Pacific variabilities that leads to SubTCP warming. In addition, the lag correlation was strongest with a lag of 5 and 6 months, indicating that a positive PDO event during boreal spring generally leads to robust SubTCP warming during the boreal summer or fall. This delayed SubTCP warming associated with the PDO might be a reason for the strong drought signal in the Korean Peninsula during the boreal summer in 2014, 2015, and 2017 (Fig. 4a).

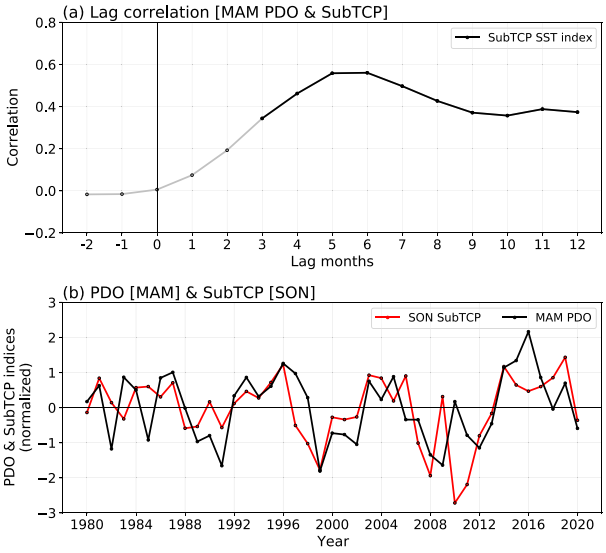

FIG. 10. (a) Lag correlation between the monthly PDO index during MAM and monthly SubTCP SST anomalies; positive lag denotes the SubTCP index is lagged by PDO index. The black line indicates a correlation coefficient over the 95% confidence level, while the gray line indicates otherwise. (b) Time series of MAM PDO index (black) and SON SubTCP index (red) during 1980–2020.

Second, PDO events are often sustained for multiple years, which helps to maintain SubTCP warming for multiple years. Figure 10b confirms that most of the SubTCP warming during the SON season was sustained for more than 2 years (e.g., 1984–87, 1992–96, 2003–06, and 2014–19) along with the multiyear PDO signal. In particular, the multiyear persistency of SubTCP warming along with the positive PDO index is evident during two longest drought events over the Korean Peninsula since 1980 (i.e., 1994–97 and 2013–17), even though a few exceptional cases without the precipitation deficit (e.g., 2003–06). This means that, even though SubTCP warming is a direct cause of the drought signal over the Korean Peninsula, the PDO contributes to sustaining SubTCP warming for multiple years, allowing SubTCP warming to cause a multiyear precipitation deficit over the Korean Peninsula. As a result, both PDO and SubTCP warming contributed to the 2013–17 drought event in the Korean Peninsula.

To examine the role of the SubTCP SST during boreal summer and fall, when the SubTCP warming associated with the positive PDO index tends to be enhanced, Figs. 11 and 12 show the regressed SST, 850-hPa streamfunction, and precipitation with respect to the SubTCP index during JJA and SON, respectively. The positive SST anomalies over the subtropical central Pacific are clearly visible, as are the local positive precipitation anomalies, indicating that the cyclonic flow over the entire North Pacific is a Gill-type response. The northerly wind anomalies, evident at the western edge of this large-scale cyclonic flow, lead a negative moisture

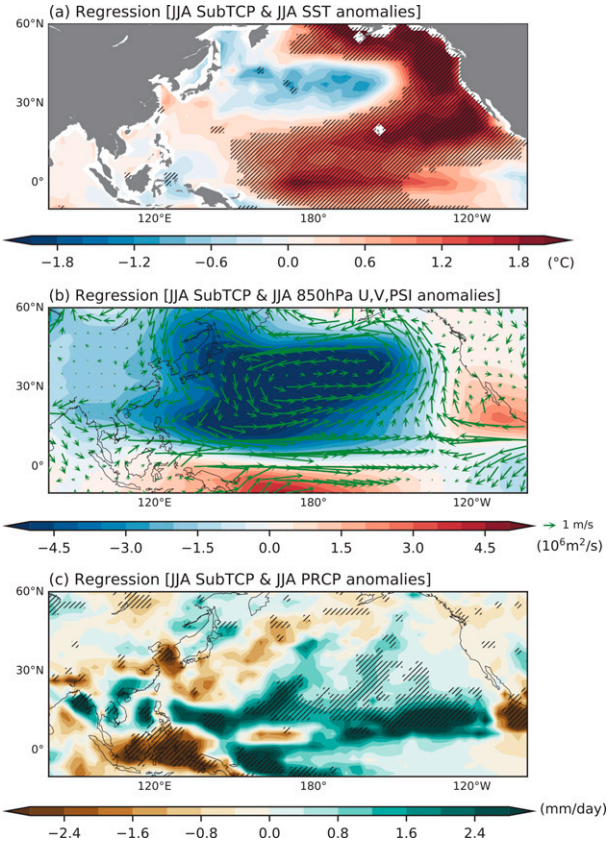

FIG. 11. Regression of (a) SST, (b) 850-hPa horizontal wind vector and streamfunction, and (c) precipitation anomalies during JJA with respect to the SubTCP index during JJA. The hatched areas in (a) and (c) denote a regression coefficient over the 95% confidence level.

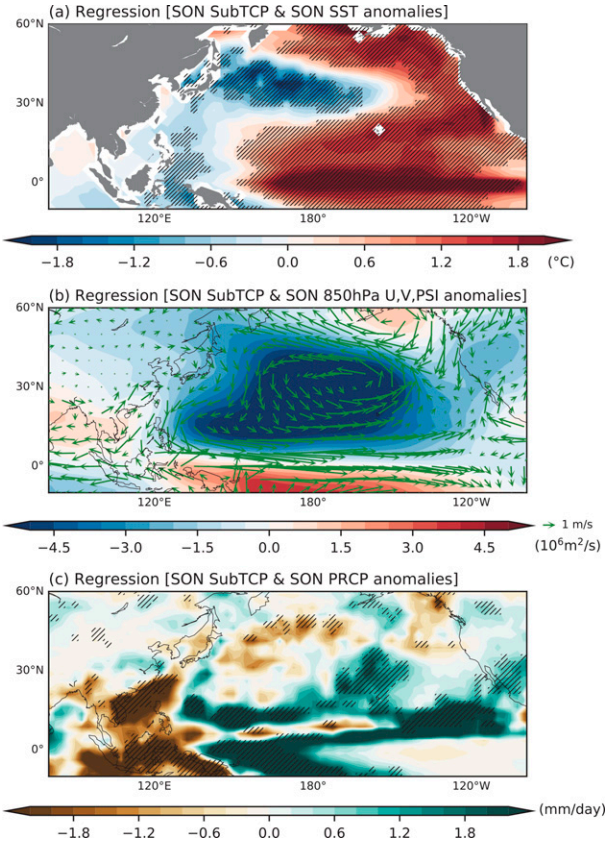

FIG. 12. As in Fig. 11, but for SON.

advection to decrease the amount of precipitation over the Korean Peninsula, Japan, and the East China Sea. The overall pattern is quite similar for the lag-regressed fields during SON (Fig. 12), supporting our argument that SubTCP warming can lead to a drought signal over the Korean Peninsula throughout the year.

6. CESM2 LE simulations

To support the main findings of section 5, we analyzed the CESM2 LE simulations. As mentioned in section 2b, we defined 5-yr drought cases in the CESM2 LE simulation. Figure 13 shows the spatial distribution of SST anomalies during the 5-yr drought events in East Asia in the CESM2 LE. The equatorial SST anomalies exhibited a La Niña signal during the first and fourth year of the 5-yr droughts, and exhibited an El Niño signal in the second and fifth year. This indicates that the equatorial SST anomalies did not exhibit any persistent features. On the other hand, the dipole pattern of the SST anomalies, which show positive and negative values over the eastern and central North Pacific, respectively, persisted for 3 years with a lag from +27 to +58 months. Consistently, the PDO index is relatively weak during the first year, and then exhibits positive values after a lag of +18 months (black line in Fig. 14).

More importantly, SST warming over the subtropical central Pacific was maintained for 5 years, which supports the observational findings. The SubTCP index during the modeled multiyear drought events showed positive values during the entire drought period, except for small negative values between the +8- and +10-month lags, and between the +24- and +28-month lags (red line in Fig. 14). Subtropical central Pacific warming was evident in the first year of the multiyear drought when the positive PDO signal was not clear, supporting our notion that subtropical central Pacific warming was a direct cause of the multiyear drought event in the Korean Peninsula.

The atmospheric teleconnection patterns, led by the positive PDO-related dipole SST anomalies over the North Pacific and SubTCP warming, were also evident in the CESM2 LE simulations (Fig. 15). SubTCP warming increased precipitation over the subtropical western-central Pacific, which led to large-scale cyclonic circulation over the western Pacific. Over the western edge of this cyclonic circulation, northerly winds were induced, leading to the horizontal advection of the cold, dry air from the north and eventually inducing the drought signal over East Asia. This supports the hypothesis that SubTCP SST warming, and the associated large-scale responses, are responsible for the multiyear drought events in the Korean Peninsula.

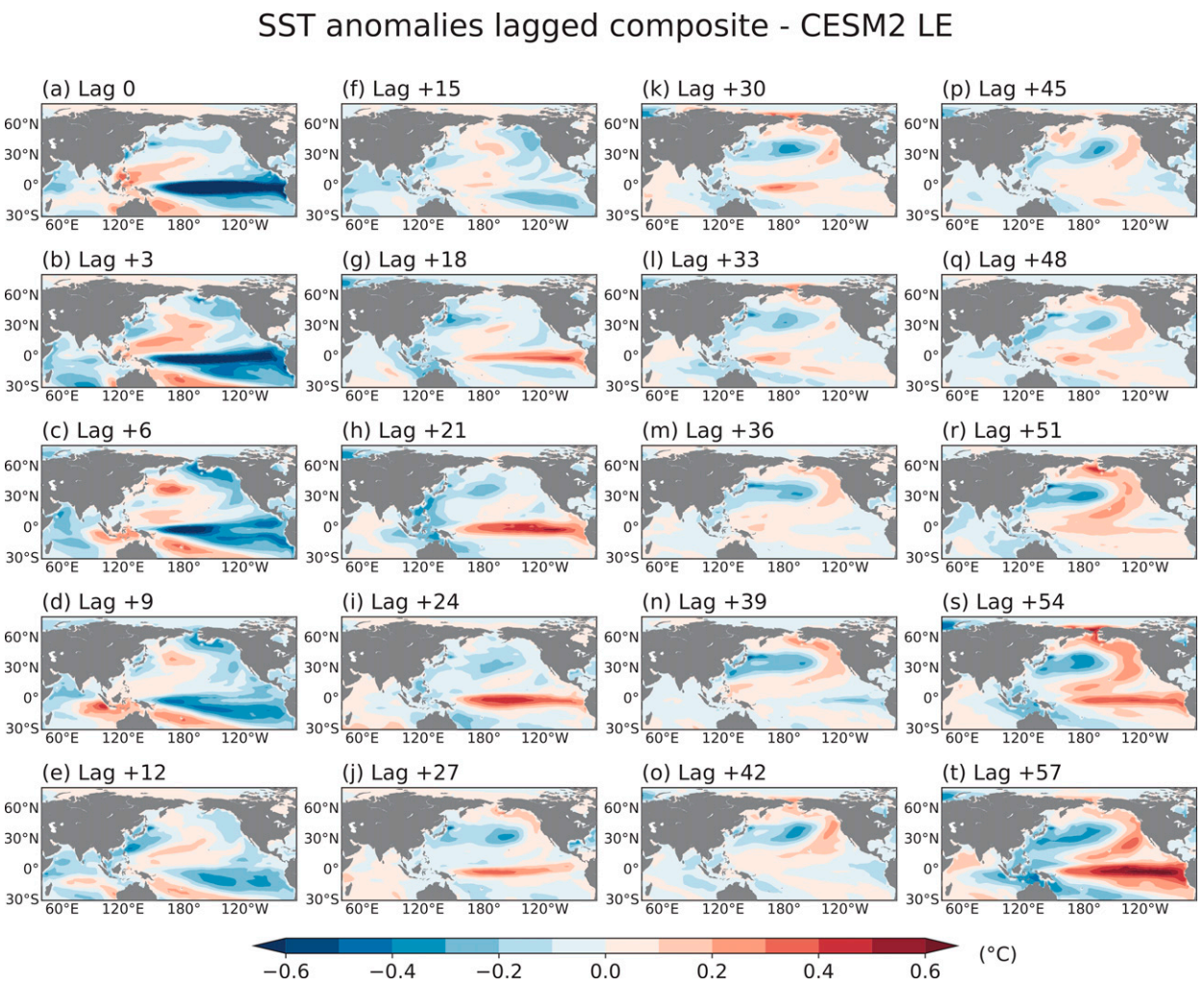

FIG. 13. Lag-composited SST anomalies with +0 to +57 months of lag after the initiation of the 5-yr drought events in CESM2 LE.

7. Summary and discussion

This study examined the contribution of PDO-related SST anomalies to the record-breaking 2013–17 drought in the Korean Peninsula. Although the drought signals in 2013 and 2016 co-occurred with heat waves, the mechanism of which is relatively well known, the cause of the 5-yr persistent precipitation deficit and the drought signals in the remaining years (i.e., 2014, 2015, and 2017) was elusive. We found that the positive PDO event persisted for more than 5 years from the mid-2010s, and the PDO-related positive SST anomalies over the subtropical central Pacific contributed to the drought signal over the Korean Peninsula in 2014, 2015, and 2017.

The SST anomalies over the southern end of the horseshoe pattern of positive SST anomalies during the positive PDO event led to an increase in the local precipitation anomalies. The enhanced atmospheric heating anomalies over the subtropical central Pacific led to a Gill-type low-atmospheric cyclonic flow centered over the North Pacific. The northerly wind at the western edge of this low-level cyclonic flow was responsible for the negative horizontal advection of moist energy, eventually contributing to decreased precipitation and resulting in a negative SPI over the Korean Peninsula in 2014, 2015, and 2017. The CESM2 LE simulation supports the observational findings that the simulated SST anomalies during the 5-yr persistent droughts also exhibited prominent SST warming over the subtropical central Pacific, along with large-scale cyclonic flow over the North Pacific.

It should be determined whether SPI-based meteorological drought was propagated by the soil moisture drought during 2013–17 (Van Loon and Laaha 2015). Surprisingly, the time series of total soil column moisture (SM) anomalies (2.89 m of soil depth) over South Korea (i.e., 32°–38°N, 135°–140°E), obtained from ERA5 (Fig. 16), shows that the amplitude of the SM deficit during 2013–17 was relatively weak compared to the precipitation deficit. For example, the SM deficit during 2013–17 was even weaker than that in other drought events (e.g., 1988, 1994–96, 2001–02, and 2008–09). Moreover, while the precipitation deficit during the 2013–17 drought is comparable, and the near-surface temperature is systematically higher to that during 1994–96, the SM deficit was much

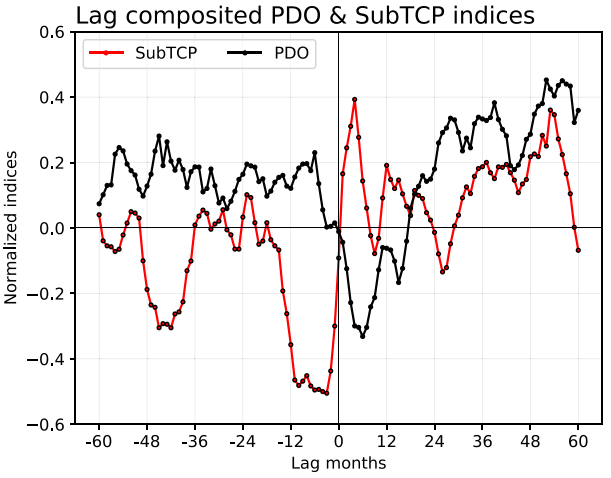

FIG. 14. Lag-composited normalized PDO (black) and SubTCP (red) indices from −60 to +60 months during the 5-yr drought events simulated in CESM2 LE.

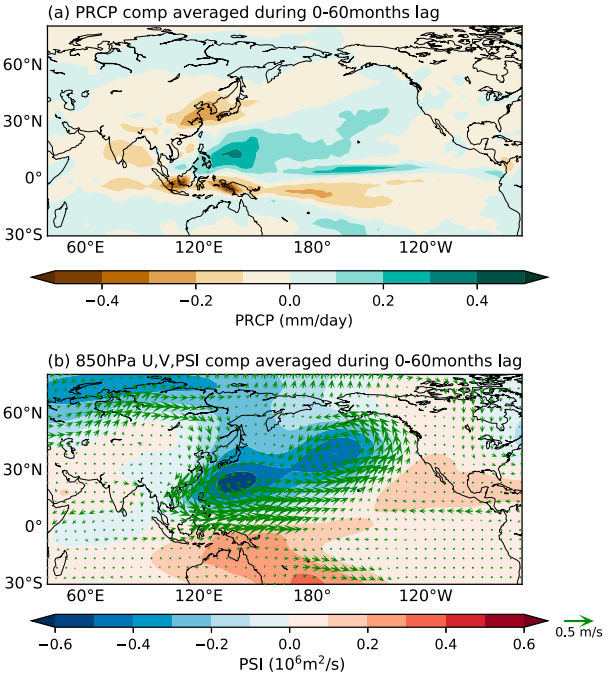

FIG. 15. The 5-yr-averaged (i.e., averaged from +0- to +60-month lag) (a) precipitation and (b) 850-hPa wind vector (arrows) and streamfunction (shading) anomalies composited during the 5-yr drought events simulated in CESM2 LE.

weaker (Fig. 16b). This indicates that the land–atmosphere coupling process, especially triggered by SM deficit, may not have been active during the 2013–17 drought.

Even though our focus was on the multiyear drought event in the Korean Peninsula during 2013–17, our findings can be applied to study other multiyear drought events. Indeed, we found that the second longest drought event (1994–96) also co-occurred with positive PDO events (Fig. 10b). The further analysis of past drought events is important for generalizing the relationship between PDO (or the SubTCP warming) and multiyear drought events in the Korean Peninsula.

The role of PDO-related SST anomalies in these multiyear drought events implies that multiyear droughts in the Korean Peninsula might be predictable to some extent (Seager et al. 2015). Mochizuki et al. (2010) showed that hindcasts of the oceanic temperature for the twentieth century exhibited reliable forecasts for predicting the PDO index for almost a decade in advance. Even though they did not evaluate the decadal forecast results initiated in 2005 due to the lack of corresponding observations, they predicted a positive PDO event in the mid-2010s [see Fig. 3b in Mochizuki et al. (2010)]. Therefore, it might be possible to predict the occurrence of multiyear drought events in the Korean Peninsula years in advance. Thus, the predictability

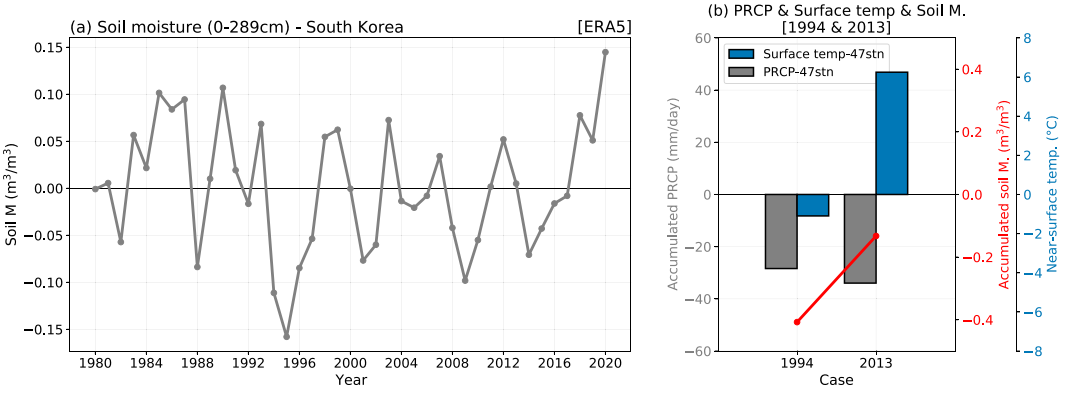

FIG. 16. (a) Time series of the detrended annual-mean soil moisture anomalies over the Korean Peninsula (32°–38°N, 135°–140°E) during 1980–2020. Note that the vertically averaged soil moisture from the surface to the deepest soil layer (i.e., 2.89 m) provided by ERA5 is shown. (b) The precipitation (gray bar), near-surface temperature (blue bar), and soil moisture anomalies (red line) for two multiyear drought cases during 1994–96 and 2013–17 in the Korean Peninsula. The definition of multiyear drought and its duration year is based on the annual-mean station-based precipitation anomalies.

of multiyear drought events in the Korean Peninsula should be examined in future work.

Acknowledgments. This study was supported by the Korea Meteorological Administration Research and Development Program under Grant KMI2018-07010. TL was supported by NSF AGS-2006553 and NOAA NA18OAR4310298.

Data availability statement. The fifth-generation ECMWF reanalysis data that support the findings of this study are available at www.ecmwf.int/en/forecasts/datasets/reanalysis-datasets/era5. The GPCP version 2.3 precipitation data are available at https://psl.noaa.gov/data/gridded/data.gpcp.html. The in-situ precipitation and surface temperature dataset at 47 stations over South Korea are available at https://data.kma.go.kr/resources/html/en/aowdp.html. The CESM2 Large Ensemble Community Project dataset are available at https://www.cesm.ucar.edu/projects/community-projects/LENS2/.

REFERENCES

Adler, R. F., and Coauthors, 2018: The Global Precipitation Climatology Project (GPCP) monthly analysis (new version 2.3) and a review of 2017 global precipitation. *Atmosphere*, **9**, 138, https://doi.org/10.3390/atmos9040138.

Bang, N. K., W. H. Nam, E. M. Hong, J. H. Michael, and D. S. Mark, 2018: Assessment of the meteorological characteristics and statistical drought frequency for the extreme 2017 spring drought event across South Korea. *J. Korean Soc. Agric. Eng.*, **60**, 37–48, https://doi.org/10.5389/KSAE.2018.60.4.037.

Boer, M. M., V. R. de Dios, and R. A. Bradstock, 2020: Unprecedented burn area of Australian mega forest fires. *Nat. Climate Change*, **10**, 171–172, https://doi.org/10.1038/s41558-020-0716-1.

Capotondi, A., Deser, C., Phillips, A. S., Okumura, Y., and Larson, S. M., 2020: ENSO and Pacific decadal variability in the Community Earth System Model version 2. *J. Adv. Model. Earth Syst.*, **12**, e2019MS002022, https://doi.org/10.1029/2019MS002022.

Chang, P., and Coauthors, 2007: Pacific meridional mode and El Niño–Southern Oscillation. *Geophys. Res. Lett.*, **34**, L16608, https://doi.org/10.1029/2007GL030302.

Chiang, J. C., and D. J. Vimont, 2004: Analogous Pacific and Atlantic meridional modes of tropical atmosphere–ocean variability. *J. Climate*, **17**, 4143–4158, https://doi.org/10.1175/JCLI4953.1.

Cook, E. R., K. J. Anchukaitis, B. M. Buckley, R. D. D'Arrigo, G. C. Jacoby, and W. E. Wright, 2010: Asian monsoon failure and megadrought during the last millennium. *Science*, **328**, 486–489, https://doi.org/10.1126/science.1185188.

Danabasoglu, G., and Coauthors, 2020: The Community Earth System Model version 2 (CESM2). *J. Adv. Model. Earth Syst.*, **12**, e2019MS001916, https://doi.org/10.1029/2019MS001916.

Deng, G., H. Zhang, X. Guo, and H. Ying, 2018: Assessment of drought in Democratic People's Republic of Korea in 2017 using TRMM data. *2018 Fifth Int. Workshop on Earth Observation and Remote Sensing Applications (EORSA)*, Xi'an, China, IEEE, 1–5, https://doi.org/10.1109/EORSA.2018.8598557.

Di Lorenzo, E., and N. Mantua, 2016: Multi-year persistence of the 2014/15 North Pacific marine heatwave. *Nat. Climate Change*, **6**, 1042–1047, https://doi.org/10.1038/nclimate3082.

Ding, Q., and B. Wang, 2005: Circumglobal teleconnection in the Northern Hemisphere summer. *J. Climate*, **18**, 3483–3505, https://doi.org/10.1175/JCLI3473.1.

Dong, L., and M. J. McPhaden, 2018: Unusually warm Indian Ocean sea surface temperatures help to arrest development of El Niño in 2014. *Sci. Rep.*, **8**, 2249, https://doi.org/10.1038/s41598-018-20294-4.

Eltahir, E. A., 1998: A soil moisture–rainfall feedback mechanism: 1. Theory and observations. *Water Resour. Res.*, **34**, 765–776, https://doi.org/10.1029/97WR03499.

Findell, K. L., and E. A. Eltahir, 1997: An analysis of the soil moisture–rainfall feedback, based on direct observations from Illinois. *Water Resour. Res.*, **33**, 725–735, https://doi.org/10.1029/96WR03756.

Fischer, E. M., S. I. Seneviratne, D. Lüthi, and C. Schär, 2007: Contribution of land–atmosphere coupling to recent European summer heat waves. *Geophys. Res. Lett.*, **34**, L06707, https://doi.org/10.1029/2006GL029068.

Folland, C. K., J. Knight, H. W. Linderholm, D. Fereday, S. Ineson, and J. W. Hurrell, 2009: The summer North Atlantic Oscillation: Past, present, and future. *J. Climate*, **22**, 1082–1103, https://doi.org/10.1175/2008JCLI2459.1.

Gill, A. E., 1980: Some simple solutions for heat. *Quart. J. Roy. Meteor. Soc.*, **106**, 447–462, https://doi.org/10.1002/qj.49710644905.

Ha, K. J., S. S. Lee, P. N. Vinayachandran, and J. G. Jhun, 2010: Changma and shifting peak in summer rainfall of Korea: ENSO influence. *Atmospheric Science*, Vol. 16, *Advances in Geosciences*, World Scientific, 35–45, https://www.worldscientific.com/doi/abs/10.1142/9789812838100_0004.

Ham, Y. G., J. S. Kug, and I. S. Kang, 2007: Role of moist energy advection in formulating anomalous Walker circulation associated with El Niño. *J. Geophys. Res.*, **112**, D24105, https://doi.org/10.1029/2007JD008744.

——, ——, S. W. Yeh, and M. Kwon, 2016: Impact of two distinct teleconnection patterns induced by western central Pacific SST anomalies on Korean temperature variability during the early boreal summer. *J. Climate*, **29**, 743–759, https://doi.org/10.1175/JCLI-D-15-0406.1.

——, Y. Chikamoto, J. S. Kug, M. Kimoto, and T. Mochizuki, 2017: Tropical Atlantic–Korea teleconnection pattern during boreal summer season. *Climate Dyn.*, **49**, 2649–2664, https://doi.org/10.1007/s00382-016-3474-z.

——, Y. Hwang, Y. K. Lim, and M. Kwon, 2018: Inter-decadal variation of the tropical Atlantic–Korea (TA-K) teleconnection pattern during boreal summer season. *Climate Dyn.*, **51**, 2609–2621, https://doi.org/10.1007/s00382-017-4031-0.

Hayes, M. J., M. D. Svoboda, D. A. Wilhite, and O. V. Vanyarkho, 1999: Monitoring the 1996 drought using the standardized precipitation index. *Bull. Amer. Meteor. Soc.*, **80**, 429–438, https://doi.org/10.1175/1520-0477(1999)080<0429:MTDUTS>2.0.CO;2.

Hersbach, H., B. Bell, P. Berrisford, S. Hirahara, and A. Horányi, 2020: The ERA5 global reanalysis. *Quart. J. Roy. Meteor. Soc.*, **146**, 1999–2049, https://doi.org/10.1002/qj.3803.

Hoerling, M., and A. Kumar, 2003: The perfect ocean for drought. *Science*, **299**, 691–694, https://doi.org/10.1126/science.1079053.

——, and Coauthors, 2014: Causes and predictability of the 2012 Great Plains drought. *Bull. Amer. Meteor. Soc.*, **95**, 269–282, https://doi.org/10.1175/BAMS-D-13-00055.1.

Hu, S., and A. V. Fedorov, 2016: Exceptionally strong easterly wind burst stalling El Niño of 2014. *Proc. Natl. Acad. Sci. USA*, **113**, 2005–2010, https://doi.org/10.1073/pnas.1514182113.

Jin, Y. H., A. Kawamura, K. Jinno, and R. Berndtsson, 2005: Detection of ENSO. *Hydrol. Processes*, **19**, 4081–4092, https://doi.org/10.1002/hyp.5873.

Kim, J.-S., and J. S. Kug, 2019: Role of off-equatorial SST in El Niño teleconnection to East Asia during El Niño decaying spring. *Climate Dyn.*, **52**, 7293–7308, https://doi.org/10.1007/s00382-016-3473-0.

Kim, J.-W., and J.-Y. Yu, 2020: Understanding reintensified multi-year El Niño events. *Geophys. Res. Lett.*, **47**, e2020GL087644, https://doi.org/10.1029/2020GL087644.

——, S.-W. Yeh, and E.-C. Chang, 2014: Combined effect of El Niño–Southern Oscillation and Pacific Decadal Oscillation on the East Asian winter monsoon. *Climate Dyn.*, **42**, 957–971, https://doi.org/10.1007/s00382-013-1730-z.

Kim, S., and J. S. Kug, 2021: Delayed impact of Indian Ocean warming on the East Asian surface temperature variation in boreal summer. *J. Climate*, **34**, 3255–3270, https://doi.org/10.1175/JCLI-D-20-0691.1.

Klein, S. A., B. J. Soden, and N. C. Lau, 1999: Remote sea surface temperature variations during ENSO: Evidence for a tropical atmospheric bridge. *J. Climate*, **12**, 917–932, https://doi.org/10.1175/1520-0442(1999)012<0917:RSSTVD>2.0.CO;2.

Kogan, F., and W. Guo, 2015: 2006–2015 mega-drought in the western USA and its monitoring from space data. *Geomatics Nat. Hazards Risk*, **6**, 651–668, https://doi.org/10.1080/19475705.2015.1079265.

Kosaka, Y., and H. Nakamura, 2006: Structure and dynamics of the summertime Pacific–Japan teleconnection pattern. *Quart. J. Roy. Meteor. Soc.*, **132**, 2009–2030, https://doi.org/10.1256/qj.05.204.

Kug, J.-S., M.-S. Ahn, M.-K. Sung, S.-W. Yeh, H.-S. Min, and Y.-H. Kim, 2010: Statistical relationship between two types of El Niño events and climate variation over the Korean Peninsula. *Asia-Pac. J. Atmos. Sci.*, **46**, 467–474, https://doi.org/10.1007/s13143-010-0027-y.

Kwon, H. H., U. Lall, and S. J. Kim, 2016: The unusual 2013–2015 drought in South Korea in the context of a multicentury precipitation record: Inferences from a nonstationary, multivariate, Bayesian copula model. *Geophys. Res. Lett.*, **43**, 8534–8544, https://doi.org/10.1002/2016GL070270.

Lee, J. H., and P. Y. Julien, 2016: ENSO impacts on temperature over South Korea. *Int. J. Climatol.*, **36**, 3651–3663, https://doi.org/10.1002/joc.4581.

Lee, S.-H., K.-H. Seo, and M. Kwon, 2019: Combined effects of El Niño and the Pacific decadal oscillation on summertime circulation over East Asia. *Asia-Pac. J. Atmos. Sci.*, **55**, 91–99, https://doi.org/10.1007/s13143-018-00103-8.

Li, T., B. Wang, C. P. Chang, and Y. Zhang, 2003: A theory for the Indian Ocean dipole–zonal mode. *J. Atmos. Sci.*, **60**, 2119–2135, https://doi.org/10.1175/1520-0469(2003)060<2119:ATFTIO>2.0.CO;2.

——, ——, B. Wu, T. Zhou, C.-P. Chang, and R. Zhang, 2018: Theories on formation of an anomalous anticyclone in western North Pacific during El Niño: A review. *J. Meteor. Res.*, **31**, 987–1006, https://doi.org/10.1007/s13351-017-7147-6.

Lim, Y. K., R. M. Kovach, S. Pawson, and G. Vernieres, 2017: The 2015/16 El Niño event in context of the MERRA-2 reanalysis: A comparison of the tropical Pacific with 1982/83 and 1997/98. *J. Climate*, **30**, 4819–4842, https://doi.org/10.1175/JCLI-D-16-0800.1.

Lu, R. Y., J. H. Oh, and B. J. Kim, 2002: A teleconnection pattern in upper-level meridional wind over the North African and Eurasian continent in summer. *Tellus*, **54A**, 44–55, https://doi.org/10.3402/tellusa.v54i1.12122.

Mantua, N. J., and S. R. Hare, 2002: The Pacific decadal oscillation. *J. Oceanogr.*, **58**, 35–44, https://doi.org/10.1023/A:1015820616384.

——, ——, Y. Zhang, J. M. Wallace, and R. C. Francis, 1997: A Pacific interdecadal climate oscillation with impacts on salmon production. *Bull. Amer. Meteor. Soc.*, **78**, 1069–1080, https://doi.org/10.1175/1520-0477(1997)078<1069:APICOW>2.0.CO;2.

Meehl, G. A., C. Shields, J. M. Arblaster, H. Annamalai, and R. Neale, 2020: Intraseasonal, seasonal, and interannual characteristics of regional monsoon simulations in CESM2. *J. Adv. Model. Earth Syst.*, **12**, e2019MS001962, https://doi.org/10.1029/2019MS001962.

Min, Q., J. Su, R. Zhang, and X. Rong, 2015: What hindered the El Niño pattern in 2014? *Geophys. Res. Lett.*, **42**, 6762–6770, https://doi.org/10.1002/2015GL064899.

Mo, K. C., 2011: Drought onset and recovery over the United States. *J. Geophys. Res.*, **116**, D20106, https://doi.org/10.1029/2011JD016168.

——, and D. P. Lettenmaier, 2015: Heat wave flash droughts in decline. *Geophys. Res. Lett.*, **42**, 2823–2829, https://doi.org/10.1002/2015GL064018.

Mochizuki, T., and Coauthors, 2010: Pacific decadal oscillation hindcasts relevant to near-term climate prediction. *Proc. Natl. Acad. Sci. USA*, **107**, 1833–1837, https://doi.org/10.1073/pnas.0906531107.

Myoung, B., J. Rhee, and C. Yoo, 2020: Long-lead predictions of warm season droughts in South Korea using North Atlantic SST. *J. Climate*, **33**, 4659–4677, https://doi.org/10.1175/JCLI-D-19-0082.1.

Nam, W. H., E. M. Hong, J. Y. Choi, T. Kim, M. J. Hayes, and M. D. Svoboda, 2017: Assessment of the extreme 2014–2015 drought events in North Korea using weekly standardized precipitation evapotranspiration index (SPEI). *J. Korean Soc. Agric. Eng.*, **59**, 65–74, https://doi.org/10.5389/KSAE.2017.59.4.065.

Newman, M., A. T. Wittenberg, L. Cheng, G. P. Compo, and C. A. Smith, 2018: The extreme 2015/16 El Niño, in the context of historical climate variability and change. *Bull. Amer. Meteor. Soc.*, **99**, S16–S20, https://doi.org/10.1175/BAMS-D-17-0116.1.

Nitta, T., 1987: Convective activities in the tropical western Pacific and their impact on the Northern Hemisphere summer circulation. *J. Meteor. Soc. Japan*, **65**, 373–390, https://doi.org/10.2151/jmsj1965.65.3_373.

Osborne, J. M., M. Collins, J. A. Screen, S. I. Thomson, and N. Dunstone, 2020: The North Atlantic as a driver of summer atmospheric circulation. *J. Climate*, **33**, 7335–7351, https://doi.org/10.1175/JCLI-D-19-0423.1.

Pal, J. S., and E. A. B. Eltahir, 2001: Pathways relating soil moisture conditions to future summer rainfall with a model of the land–atmosphere system. *J. Climate*, **14**, 1227–1242, https://doi.org/10.1175/1520-0442(2001)014<1227:PRSMCT>2.0.CO;2.

Park, C. K., C. H. Ho, D. S. R. Park, T. W. Park, and J. Kim, 2020: Interannual variations of spring drought-prone conditions over three subregions of East Asia and associated large-scale circulations. *Theor. Appl. Climatol.*, **142**, 1117–1131, https://doi.org/10.1007/s00704-020-03371-5.

Peng, J.-B., 2014: An investigation of the formation of the heat wave in southern China in summer 2013 and the relevant abnormal subtropical high activities. *Atmos. Oceanic Sci. Lett.*, **7**, 286–290, https://doi.org/10.3878/j.issn.1674-2834.13.0097.

Peters, A. J., E. Walter-Shea, A. Vina, M. Hayes, and M. D. Svoboda, 2002: Drought monitoring with NDVI-based standardized vegetation index. *Photogramm. Eng. Remote Sens.*, **68**, 71–75.

Press, W. H., W. T. Vetterling, S. A. Teukolsky, and B. P. Flannery, 1986: *Numerical Recipes*. Cambridge University Press, 123–128.

Rodgers, K. B., and Coauthors, 2021: Ubiquity of human-induced changes in climate variability. *Earth Syst. Dyn.*, **12**, 1393–1411, https://doi.org/10.5194/esd-12-1393-2021.

Roundy, J. K., C. R. Ferguson, and E. F. Wood, 2013: Temporal variability of land–atmosphere coupling and its implications for drought over the southeast United States. *J. Hydrometeor.*, **14**, 622–635, https://doi.org/10.1175/JHM-D-12-090.1.

Santanello, J. A., C. D. Peters-Lidard, and S. V. Kumar, 2011: Diagnosing the sensitivity of local land–atmosphere coupling via the soil moisture–boundary layer interaction. *J. Hydrometeor.*, **12**, 766–786, https://doi.org/10.1175/JHM-D-10-05014.1.

Sattar, M. N., J. Y. Lee, J. Y. Shin, and T. W. Kim, 2019: Probabilistic characteristics of drought propagation from meteorological to hydrological drought in South Korea. *Water Resour. Manage.*, **33**, 2439–2452, https://doi.org/10.1007/s11269-019-02278-9.

Schubert, S. D., M. J. Suarez, P. J. Pegion, R. D. Koster, and J. T. Bacmeister, 2008: Potential predictability of long-term drought and pluvial conditions in the United States Great Plains. *J. Climate*, **21**, 802–816, https://doi.org/10.1175/2007JCLI1741.1.

——, H. Wang, and M. Suarez, 2011: Warm season subseasonal variability and climate extremes in the Northern Hemisphere: The role of stationary Rossby waves. *J. Climate*, **24**, 4773–4792, https://doi.org/10.1175/JCLI-D-10-05035.1.

——, ——, R. D. Koster, M. J. Suarez, and P. Ya. Groisman, 2014: Northern Eurasian heat waves and droughts. *J. Climate*, **27**, 3169–3207, https://doi.org/10.1175/JCLI-D-13-00360.1.

Seager, R., and M. Hoerling, 2014: Atmosphere and ocean origins of North American droughts. *J. Climate*, **27**, 4581–4606, https://doi.org/10.1175/JCLI-D-13-00329.1.

——, A. Tzanova, and J. Nakamura, 2009: Drought in the southeastern United States: Causes, variability over the last millennium, and the potential for future hydroclimate change. *J. Climate*, **22**, 5021–5045, https://doi.org/10.1175/2009JCLI2683.1.

——, and Coauthors, 2015: Causes of the 2011–14 California drought. *J. Climate*, **28**, 6997–7024, https://doi.org/10.1175/JCLI-D-14-00860.1.

Simpson, I. R., and Coauthors, 2020: An evaluation of the large-scale atmospheric circulation and its variability in CESM2 and other CMIP models. *J. Geophys. Res. Atmos.*, **125**, e2020JD032835, https://doi.org/10.1029/2020JD032835.

Son, H.-Y., J.-Y. Park, J.-S. Kug, J. Yoo, and C.-H. Kim, 2014: Winter precipitation variability over Korean Peninsula associated with ENSO. *Climate Dyn.*, **42**, 3171–3186, https://doi.org/10.1007/s00382-013-2008-1.

——, ——, and ——, 2016: Precipitation variability in September over the Korean Peninsula during ENSO developing phase. *Climate Dyn.*, **46**, 3419–3430, https://doi.org/10.1007/s00382-015-2776-x.

Sung, M.-K., W.-T. Kwon, H.-J. Baek, K.-O. Boo, G.-H. Lim, and J.-S. Kug, 2006: A possible impact of the North Atlantic Oscillation on the East Asian summer monsoon precipitation. *Geophys. Res. Lett.*, **33**, L21713, https://doi.org/10.1029/2006GL027253.

Van Loon, A. F., and G. Laaha, 2015: Hydrological drought severity explained by climate and catchment characteristics. *J. Hydrol.*, **526**, 3–14, https://doi.org/10.1016/j.jhydrol.2014.10.059.

Vautard, R., and Coauthors, 2007: Summertime European heat and drought waves induced by wintertime Mediterranean rainfall deficit. *Geophys. Res. Lett.*, **34**, L07711, doi:10.1029/2006GL028001.

Wallace, J. M., and D. S. Gutzler, 1981: Teleconnections in the geopotential height field during the Northern Hemisphere winter. *Mon. Wea. Rev.*, **109**, 784–812, https://doi.org/10.1175/1520-0493(1981)109<0784:TITGHF>2.0.CO;2.

Wang, B., R. Wu, and X. Fu, 2000: Pacific–East Asian teleconnection: How does ENSO affect East Asian climate? *J. Climate*, **13**, 1517–1536, https://doi.org/10.1175/1520-0442(2000)013<1517:PEATHD>2.0.CO;2.

——, J. Liu, J. Yang, T. Zhou, and Z. Wu, 2009: Distinct principal modes of early and late summer rainfall anomalies in East Asia. *J. Climate*, **22**, 3864–3875, https://doi.org/10.1175/2009JCLI2850.1.

Wang, H., and S. Schubert, 2014: Causes of the extreme dry conditions over California during early 2013 [in "Explaining Extreme Events of 2013 from a Climate Perspective"]. *Bull. Amer. Meteor. Soc.*, **95** (9), S7–S11, https://doi.org/10.1175/1520-0477-95.9.S1.1.

——, and S. He, 2015: The north China/northeastern Asia severe summer drought in 2014. *J. Climate*, **28**, 6667–6681, https://doi.org/10.1175/JCLI-D-15-0202.1.

Wang, L., and X. Yuan, 2018: Two types of flash drought and their connections with seasonal drought. *Adv. Atmos. Sci.*, **35**, 1478–1490, https://doi.org/10.1007/s00376-018-8047-0.

Wang, S., X. Yuan, and Y. Li, 2017: Does a strong El Niño imply a higher predictability of extreme drought? *Sci. Rep.*, **7**, 40741, https://doi.org/10.1038/srep40741.

Wang, S. Y. S., and Coauthors, 2015: An intensified seasonal transition in the Central U.S. that enhances summer drought. *J. Geophys. Res. Atmos.*, **120**, 8804–8816, https://doi.org/10.1002/2014JD023013.

Wu, B., T. Li, and T. Zhou, 2010: Relative contributions of the Indian Ocean and local SST anomalies to the maintenance of the western North Pacific anomalous anticyclone during the El Niño decaying summer. *J. Climate*, **23**, 2974–2986, https://doi.org/10.1175/2010JCLI3300.1.

Wu, R., and J. L. Kinter III, 2009: Analysis of the relationship of U.S. droughts with SST and soil moisture: Distinguishing the time scale of droughts. *J. Climate*, **22**, 4520–4538, https://doi.org/10.1175/2009JCLI2841.1.

Xia, J., K. Tu, Z. Yan, and Y. Qi, 2016: The super-heat wave in eastern China during July–August 2013: A perspective of climate change. *Int. J. Climatol.*, **36**, 1291–1298, https://doi.org/10.1002/joc.4424.

Xie, S. P., H. Annamalai, F. A. Schott, and J. P. McCreary Jr., 2002: Structure and mechanisms of South Indian Ocean climate variability. *J. Climate*, **15**, 864–878, https://doi.org/10.1175/1520-0442(2002)015<0864:SAMOSI>2.0.CO;2.

Yeh, S. W., Y. J. Won, J. S. Hong, K. J. Lee, M. Kwon, K. H. Seo, and Y. G. Ham, 2018: The record-breaking heat wave in 2016 over South Korea and its physical mechanism. *Mon. Wea. Rev.*, **146**, 1463–1474, https://doi.org/10.1175/MWR-D-17-0205.1.

Yeo, S. R., S. W. Yeh, and W. S. Lee, 2019: Two types of heat wave in Korea associated with atmospheric circulation pattern. *J. Geophys. Res. Atmos.*, **124**, 7498–7511, https://doi.org/10.1029/2018JD030170.

Zeng, D., X. Yuan, and J. K. Roundy, 2019: Effect of teleconnected land–atmosphere coupling on Northeast China persistent drought in spring–summer of 2017. *J. Climate*, **32**, 7403–7420, https://doi.org/10.1175/JCLI-D-19-0175.1.

Zhang, P., and Coauthors, 2020: Abrupt shift to hotter and drier climate over inner East Asia beyond the tipping point. *Science*, **370**, 1095–1099, https://doi.org/10.1126/science.abb3368.

Zhang, W., Z. Huang, F. Jiang, M. F. Stuecker, G. Chen, and F.-F. Jin, 2021: Exceptionally persistent Madden–Julian oscillation activity contributes to the extreme 2020 East Asian summer monsoon rainfall. *Geophys. Res. Lett.*, **48**, e2020GL091588, https://doi.org/10.1029/2020GL091588.